Polym. Bull. (2011) 67:1605–1619
DOI 10.1007/s00289-011-0509-9

ORIGINAL PAPER

Polyester/natural fiber biocomposites: preparation, characterization, and biodegradability

Chin-San Wu · Fu-San Yen · Chen-Yu Wang

Received: 7 February 2011 / Revised: 9 May 2011 / Accepted: 17 May 2011 /
Published online: 24 May 2011

Abstract In this study, the biodegradability, morphology, mechanical, and thermal properties of composite materials composed of polybutyleneterephthalate (PBT), acrylic acid-grafted PBT (PBT-g-AA), and sisal fibers (SFs) were evaluated. Composites containing acrylic acid-grafted PBT (PBT-g-AA/SF) exhibited superior mechanical properties because of their greater compatibility with SF than PBT/SF. The dispersion of SF in the PBT-g-AA matrix was highly homogeneous due to ester formation and the creation of branched and cross-linked macromolecules between the carboxyl groups of PBT-g-AA and the hydroxyl groups of SF. Furthermore, due to its lower melting temperature (T_m), the PBT-g-AA/SF composite was more readily synthesized. Each composite was subjected to biodegradation tests in a soil environment. Both the PBT and PBT-g-AA/SF composite films were completely degraded, with severe disruption of the film structures observed after 60–100 days of incubation. Although the degree of weight loss following burial indicated that both materials were biodegradable, even with high levels of SF loading, the higher water resistance of PBT-g-AA/SF films indicated their higher biodegradability than the PBT films.

Keywords Biocomposites · Poly(butylene terephthalate) · Biodegradability · Sisal fiber

C.-S. Wu (✉) · C.-Y. Wang
Department of Chemical and Biochemical Engineering, Kao Yuan University,
82101 Kaohsiung County, Taiwan, ROC
e-mail: t50008@cc.kyu.edu.tw

F.-S. Yen
Department of Chemical and Material Engineering, National Kaohsiung University of Applied Sciences, 807 Kaohsiung County, Taiwan, ROC

Introduction

As industry attempts to lessen the dependence on petroleum-based fuels and products, there is an increasing need to investigate more environmentally friendly, sustainable materials. These include biodegradable polyesters from renewable or fossil sources, or a combination of both to replace existing materials that present numerous economic and environmental issues, including waste management and carbon emissions [1–3]. However, due to the high cost and poor mechanical quality of aliphatic polyesters, their use has been limited in electronics and industrial and automotive production.

Aromatic polyesters are, however, commonly used in engineering, constructional, and structural applications because of their low cost, high stiffness, strength, dimensional stability, low water absorption, and favorable chemical and electrical resistance. A problem with these aromatic polyesters is that they do not biodegrade under normal environmental conditions [4, 5].

Biocomposites of thermoplastic polymers and natural fibers can completely degrade in soil or compost. The use of fiber reinforcement is an attractive method to improve the mechanical properties of biodegradable plastics [6–9]. Among these thermoplastic polyesters, PBT is a popular because it displays a high mechanical strength and modulus compared with other thermoplastic polyesters, such as PBS, PVA, and PLA. Unfortunately, PBT is expensive; however, its cost can be reduced through the blending of PBT composites with natural biomaterials. Plant fibers that increase the tensile strength of composites have recently been used as a means of reinforcing polymer matrices for replacement with synthetic fibers.

Sisal is an abundant natural fiber with excellent tensile strength that can improve the mechanical properties of materials. Moreover, although sisal fibers (SFs) range in length and require a compatibilizing agent to wet the fibers [10, 11], the highly hydrophilic nature of PBT results in the natural wetting of SF. Thus, composites of PBT and SF offer advantages in both biocompatibility and cost [12, 13].

In this report, we describe a systematic investigation of the mechanical properties and biodegradability of SF composites with PBT and acrylic acid (AA)-grafted PBT (PBT-g-AA). Composites were characterized using Fourier-transform infrared spectroscopy (FTIR) and ^{13}C nuclear magnetic resonance (NMR) to identify bulk structural changes induced by the AA moiety. In addition, the effects of the SF content on biodegradability were assessed for the PBT/SF and PBT-g-AA/SF composites. The composites were shown to be biodegradable in a soil environment. These results of this study will serve as a reference for future composites.

Experimental procedures

Materials

PBT resins (PBT-1100) were obtained from Chang Chun Corp. AA was obtained from Sigma-Aldrich (St. Louis, MO, USA) and was purified before use by

recrystallization from chloroform. Benzoyl peroxide (BPO; Sigma-Aldrich) was used as an initiator and was purified by dissolution in chloroform and reprecipitation in methanol. SF was obtained from Pingtung.

Grafting reaction and percentage

Using BPO as the initiator, AA was grafted onto molten PBT under a nitrogen atmosphere at 45 ± 2 °C with a mixer rotor speed of 60 rpm. A mixture of AA and BPO was added in four equal portions at 2-min intervals to molten PBT to allow grafting. The reactions were performed under a nitrogen atmosphere at 45 ± 2 °C. Preliminary experiments showed that reaction equilibrium was attained in less than 12 h. Thus, reactions were allowed to proceed for 12 h under stirring at a rotor speed of 60 rpm. The resulting product (4 g) was dissolved in 200 mL of refluxing $CF_3COOH/CDCl_3$ solution (20:80, v/v) at 45 ± 2 °C, and the solution was filtered through several layers of cheesecloth. The $CF_3COOH/CDCl_3$-soluble product in the filtrate was extracted five times using 600 mL of cold acetone per extraction. The AA loading of the $CF_3COOH/CDCl_3$-soluble polymer was determined by titration and expressed as a grafting percentage. Approximately 2 g of the copolymer was heated for 2 h in 200 mL of refluxing $CF_3COOH/CDCl_3$ solution. This solution was then titrated immediately with 0.03 N ethanolic KOH, which had been standardized against a solution of potassium hydrogen phthalate, using a phenolphthalein indicator. The acid number and the grafting percentage were then calculated using the following equations: [14]

$$\text{Acid number}(\text{mg KOH/g}) = \frac{\text{VKOH(mL)} \times \text{C}_{\text{KOH}}(\text{N}) \times 56.1}{\text{polymer(g)}} \quad (1)$$

$$\text{Grafting percentage}(\%) = \frac{\text{Acid number} \times 72}{561} \times 100\% \quad (2)$$

At BPO and AA loadings of 0.3 and 10 wt%, respectively, the grafting percentage was 6.76 wt%.

SF processing

SF was extracted from crushed Taiwanese sisal. As shown in Scheme 1, the purification consisted of immersing 60 g of ground and dried SF in 1000 mL of distilled water for 7 days to remove any water-soluble components. The product was then dried at 45 °C for 2 days under vacuum. After drying, 1000 mL of NaOH (0.1 M) was added to the SF, and after 2 days, the suspension was vacuum-filtered. The product was washed five times and dried at 55 °C for 2 days under vacuum. The resulting light yellow fibers were 7–9-cm long. The fibers were dried, ground, and sorted. After grinding, the fiber mixture consisted of a fine brown powder with dispersed 150–450 μm pale yellow single fibers. The samples were passed through 60-mesh (0.246 mm) and 80-mesh (0.175 mm) sieves, air-dried for 3 days at

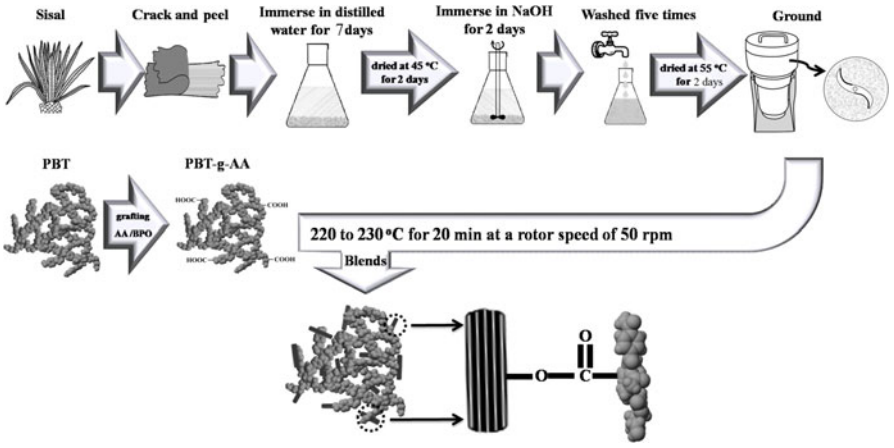

Scheme 1 Reaction scheme for the modification of PBT and SF and the preparation of composite materials

65–75 °C, and vacuum-dried for at least 5 h at 105 °C until the moisture content fell to 5 ± 1%.

Composite preparation

Before composite fabrication, SF samples were cleaned with acetone and dried in an oven at 105 °C for 24 h. Composites were prepared in a "Plastograph" 200-Nm Mixer W50EHT with a blade rotor (Brabender, Dayton, OH). The composites were mixed between 220 and 230 °C for 20 min at a rotor speed of 50 rpm. Samples were prepared with mass ratios of SF to PBT or to PBT-g-AA of 10/90, 20/80, 30/70, and 40/60. Residual AA in the PBT-g-AA reaction mixture was removed by acetone extraction before the preparation of PBT-g-AA/SF. After mixing, the composites were pressed into sheets with a hot press and placed in a dryer for cooling. These sheets were cut to standard sample dimensions for further characterization.

NMR/FTIR/TGA analyses

Solid-state ^{13}C NMR spectra were acquired with an AMX-400 NMR spectrometer at 100 MHz under cross polarization while spinning at the magic angle. Power decoupling conditions were set with a 90° pulse and a 4-s cycle time. Infrared spectra of the samples were obtained using a Bio-Rad FTS-7PC FTIR spectrophotometer. Thermogravimetric analysis (TA Instrument 2010 TGA, New Castle, DE) was used to assess whether the organic–inorganic phase interactions influenced the thermal degradation of the hybrids. Samples were placed in alumina crucibles and assessed with a thermal ramp over the temperature range of 30–600 °C, at a heating rate of 10 °C min^{-1}. The initial decomposition temperature (IDT) of the hybrids was obtained.

Mechanical testing

An Instron mechanical tester (Model LLOYD, LR5K type) was used to measure the tensile strength at break and flexural properties, in accordance with ASTM D638 and ASTM D790. Test samples were prepared in a hydraulic press at 230 °C and conditioned at 50 ± 5% relative humidity for 24 h before measurement. Measurements were performed using a crosshead speed of 20 mm min^{-1}. Five measurements were performed for each sample, and the mean value was determined.

Composite morphology

A thin film of each composite was created with a hydraulic press and treated with hot water at 80 °C for 24 h before gold coating. The surface morphology of the films was observed using a scanning electron microscope (SEM; Hitachi Microscopy Model S-1400, Tokyo, Japan).

Water absorption

Samples were prepared for water absorption measurements by cutting into 75 × 30-mm strips (150 ± 5-μm thick) in accordance with ASTM D570-81. The samples were dried in a vacuum oven at 50 ± 2 °C for 8 h, cooled in a desiccator, and immediately weighed to the nearest 0.001 g (W_c). The samples were then immersed in distilled water and maintained at 25 ± 2 °C for 60 days. During this time, samples were removed from the water at 10-day intervals, gently blotted with tissue paper to remove excess water from their surfaces, weighed to the nearest 0.001 g (W_w), and returned to the water. Each W_w value was the average of three measurements. The percentage weight increase due to water absorption (W_f) was calculated to the nearest 0.01% according to Eq. 1:

$$\%W_f = \frac{W_w - W_c}{W_c} \times 100\%. \quad (1)$$

Biodegradation studies

The biodegradability of the samples was assessed by measuring the weight loss of the composites over time in a soil environment. The samples measuring 35 × 25 × 1 mm^3 were weighed and buried in boxes of alluvial-type soil that had been obtained in May 2009 from farmland topsoil before planting. The soil was sifted to remove large clumps and plant debris. Procedures for soil burial were as described by Alvarez et al. [15]. The soil was maintained at approximately 35% moisture by weight, and the samples were buried at a depth of 10–12 cm. A control box consisted of samples with no soil. The buried samples were removed after 2 weeks, washed in distilled water, dried in a vacuum oven at 50 ± 2 °C for 3 days, and equilibrated in a desiccator for at least 1 day. The samples were then weighed before being returned to the soil.

Results and discussion

Structural characterization

FTIR spectra of PBT, PBT-g-AA, PBT/SF, and PBT-g-AA/SF are shown in Fig. 1. Characteristic peaks of PBT at 3200–3700, 1700–1750, and 500–1600 cm^{-1} were observed in both neat PBT and PBT-g-AA [16]. An additional peak at 1710 cm^{-1}, assigned to –C=O, and a broad O–H stretching transition at 3265 cm^{-1} were observed in the modified PBT. The shoulder near 1710 cm^{-1} was attributed to free acid in the modified polymer. This distinctive pattern of peaks indicated successful grafting of AA onto PBT, similar to previous studies [17]. The peak assigned to the O–H stretching vibration at 3200–3700 cm^{-1} intensified in the PBT/SF (20 wt%) composite (Fig. 1c) due to the contribution of the –OH group of SF. The FTIR spectrum of the PBT-g-AA/SF (20 wt%) composite in Fig. 1d revealed a peak at 1737 cm^{-1} that was not present in the FTIR spectrum of the PBT/SF (20 wt%) composite. This peak was assigned to the ester carbonyl stretching vibration of the copolymer. Shah et al. [18] also reported an absorption peak at 1735 cm^{-1} for this ester carbonyl group. These data suggest the formation of branched and cross-linked

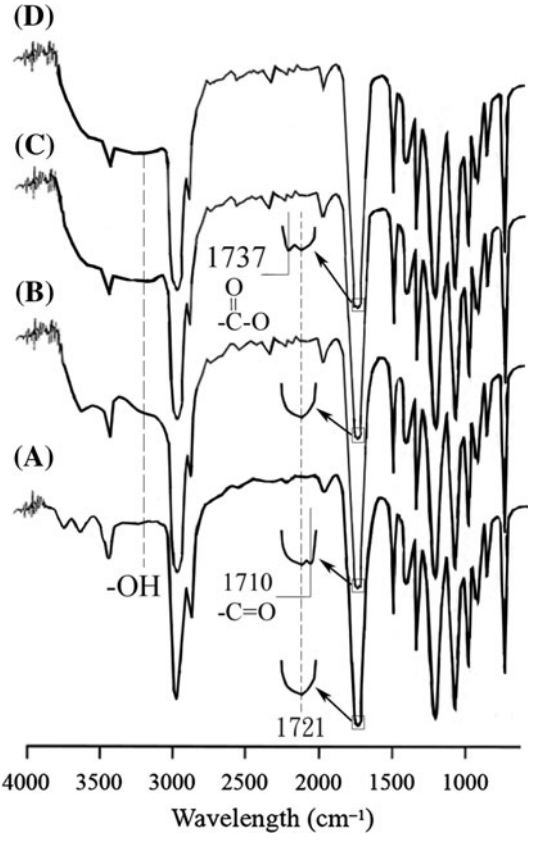

Fig. 1 FTIR spectra for (*A*) PBT, (*B*) PBT-g-AA, (*C*) PBT/SF (20 wt%), and (*D*) PBT-g-AA/SF (20 wt%)

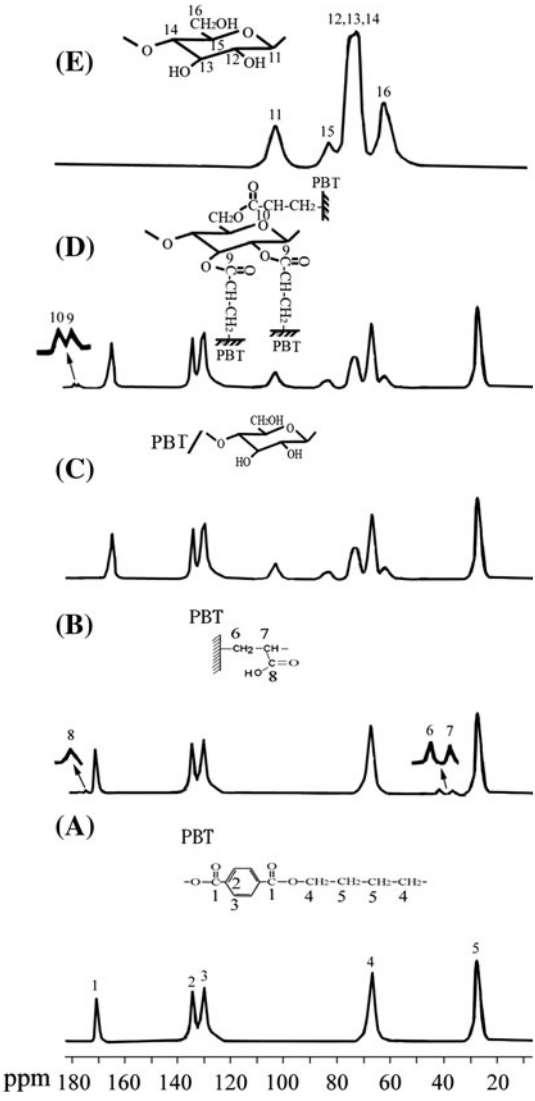

Fig. 2 Solid-state ^{13}C NMR spectra for **a** PBT, **b** PBT-g-AA, **c** PBT/SF (20 wt%), **d** PBT-g-AA/SF (20 wt%), and **e** SF

macromolecules in the PBT-g-AA/SF composite by covalent reaction of the AA carboxyl groups in PBT-g-AA with the hydroxyl groups of SF.

Further evidence for ester formation was provided by solid-state ^{13}C NMR spectroscopy. The solid-state ^{13}C NMR spectrum of neat PBT (Fig. 2a) was similar to that reported by Jansen et al. [19] and showed five peaks: 1: $\delta = 170.2$ ppm; 2: $\delta = 134.2$ ppm; 3: $\delta = 129.7$ ppm; 4: $\delta = 66.8$ ppm; and 5: $\delta = 27.9$ ppm. Compared with that of neat PBT, the ^{13}C NMR spectrum of PBT-g-AA (Fig. 3b) contained three additional peaks: 6: $\delta = 35.5$ ppm, 7: $\delta = 42.2$ ppm, and 8: $\delta = 174.8$. These peaks confirmed the grafting of AA onto PBT (Fig. 2b).

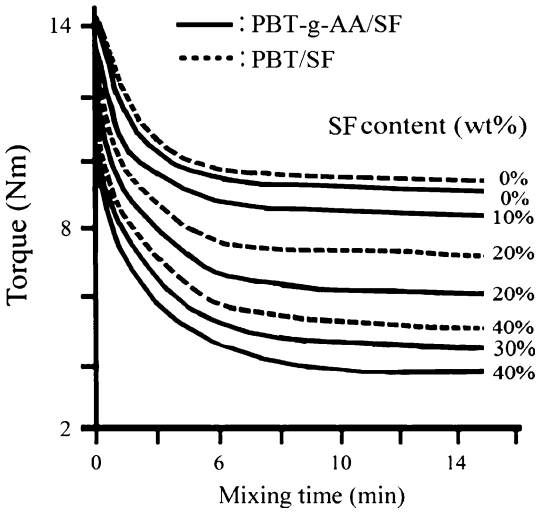

Fig. 3 Torque values plotted as a function of the mixing time for PBT/SF and PBT-g-AA/SF composites with varying SF content

The solid-state ^{13}C NMR spectra of PBT-g-AA/SF (20 wt%), PBT/SF (20 wt%), and SF are shown in Fig. 2c–e. The spectra are similar to those reported by Martins et al. [20]. Compared with unmodified PBT, additional peaks were observed in the spectra of composites containing PBT-g-AA. These additional peaks were located at $\delta = 42.2$ ppm (6) and $\delta = 35.5$ ppm (7). The same features were observed in previous studies [14] and indicate grafting of AA onto PBT. However, the peak at $\delta = 174.8$ ppm (−C=O) (8) (Fig. 2b), which is also typical for AA grafted onto PBT, was absent in the solid-state spectrum of PBT-g-AA/SF (20 wt%). This is likely the result of an additional condensation reaction between the carboxyl group of AA and the –OH group of SF that caused the peak at $\delta = 174.8$ ppm to split into two bands ($\delta = 177.1$ and 177.9 ppm). This additional reaction converted the fully acylated groups in the original SF to esters (represented by peaks 9 and 10 in Fig. 2c) and did not occur between PBT and SF, as indicated by the absence of corresponding peaks in the FTIR spectrum of PBT/SF (20 wt%) in Fig. 2d. The formation of ester groups significantly affected the thermal and biodegradation properties of PBT-g-AA/SF and is discussed in greater detail in the following sections.

Torque measurements during mixing

The effects of SF content and mixing time on the melt torque of PBT/SF and PBT-g-AA/SF composites are shown in Fig. 3. During the measurement, PBT or PBT-g-AA was initially melted at 220–230 °C. SF was then gradually added into the melt. The torque values decreased with an increasing SF content and mixing time, approaching a stable value when mixed for 8 min. The final torque values decreased with increasing SF content, because the melt viscosity of SF was lower than that of PBT or PBT-g-AA. Thus, the melt viscosity of the entire blend reduced. In addition, the melt torque values of the PBT-g-AA/SF composites were significantly lower

than those of the PBT/SF composites at the same SF content. According to Wu [21], this lowered melt viscosity was due to the formation of ester carbonyl groups, leading to conformational changes in the wood flour molecules.

Composite morphology

In most composite materials, effective wetting and uniform dispersion of all components in a given matrix and strong interfacial adhesion between the phases are required to obtain a composite with satisfactory mechanical properties. In the current study, SF may be thought of as a dispersed phase within a PBT or PBT-g-AA matrix. To evaluate the composite morphology, SEM was used to examine tensile fractures in the PBT/SF (20 wt%) and PBT-g-AA/SF (20 wt%) surfaces. The SEM images of PBT/SF (20 wt%) in Fig. 4a show that the SF in this composite tended to agglomerate into bundles and was unevenly distributed in the matrix. This poor dispersion was due to the formation of hydrogen bonds among SF fibers and the disparate hydrophilicities of PBT and SF. Poor wetting in these composites was also noted (marked in Fig. 4a) due to large differences in surface energy between the SF and the PBT matrix [22]. The PBT-g-AA/SF (20 wt%) photomicrograph in Fig. 4b shows a more homogeneous dispersion and improved SF wetting in the PBT-g-AA matrix, indicated by the complete coverage of PBT-g-AA on the fiber and the removal of both materials when a fiber was pulled from the bulk. This improved interfacial adhesion was due to a similar hydrophilicity of the two

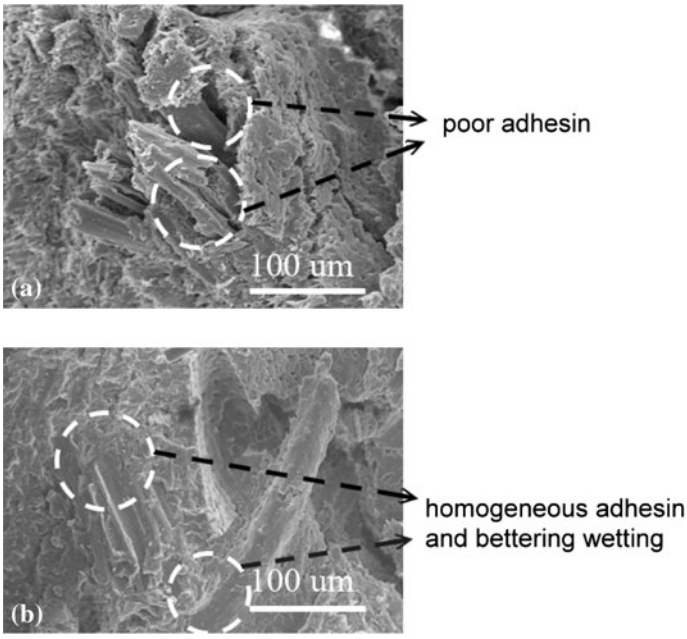

Fig. 4 SEM photomicrographs show the distribution and adhesion of SF in **a** PBT/SF (20 wt%) and **b** PBT-g-AA/SF (20 wt%) composites

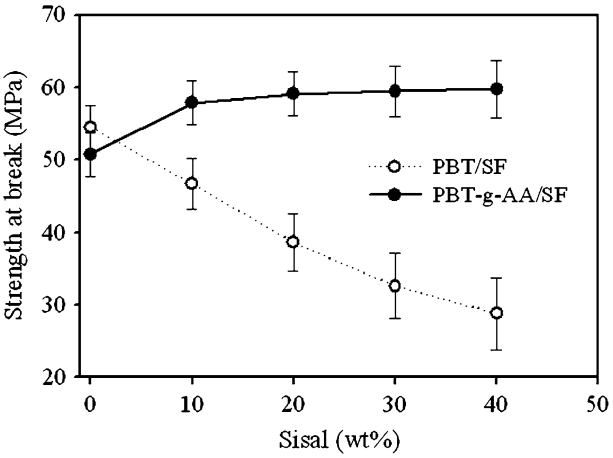

Fig. 5 Effect of the SF content on the tensile strength at break is shown for PBT/SF and PBT-g-AA/SF composites

Table 1 Effect of SF content on the flexural properties of PBT/SF and PBT-g-AA/SF composites

SF (wt%)	PBT/SF		PBT-g-AA/SF	
	E (GPa)	σ^* (MPa)[a]	*E* (GPa)	σ^* (MPa)[a]
0	2.35 ± 0.11	111.6 ± 4.6	2.22 ± 0.12	108.3 ± 4.8
10	2.02 ± 0.15	99.6 ± 4.8	2.53 ± 0.16	126.3 ± 4.3
20	1.86 ± 0.20	89.8 ± 5.1	2.63 ± 0.18	128.6 ± 4.5
30	1.68 ± 0.25	83.6 ± 5.5	2.65 ± 0.21	130.1 ± 4.6
40	1.49 ± 0.30	78.8 ± 5.9	2.68 ± 0.23	131.2 ± 4.8

[a] Stress at break for PBT, stress at yield for PBT

components, allowing the formation of branched and cross-linked macromolecules, preventing hydrogen bonding between the SF fibers.

Mechanical properties

Figure 5 and Table 1 show the variation in tensile strength at break and flexural properties with SF content for PBT/SF and PBT-g-AA/SF composites. The tensile strength of neat PBT decreased when grafted with AA. For PBT/SF composites (Fig. 5; Table 1), the tensile strength decreased continuously as the SF content increased, because of the poor dispersion of SF in the PBT matrix. This demonstrated an incompatibility between the two polymers, impacting the mechanical properties of the composite. The tensile strength of PBT-g-AA/SF was lower than that of PBT. The tensile strength increased at 10 wt% SF, due to esterification between PBT-g-AA and SF. The tensile strength decreased at high SF levels due to agglomeration and the uneven distribution of residual SF, which was

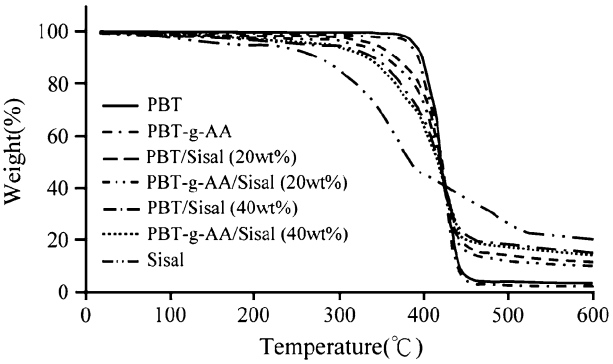

Fig. 6 Effect of the SF content on the TGA curves is shown for PBT/SF and PBT-g-AA/SF composites

Table 2 Effect of SF content on the thermal properties of PBT/SF and PBT-g-AA/SF composites

SF (wt%)	PBT/SF IDT (°C)	PBT-g-AA/SF IDT (°C)
0	393	387
10	362	369
20	343	349
30	336	341
40	325	330

present because of the low grafting level, 6.76%. Furthermore, it was found that the PBT-g-AA/SF composites not only gave higher tensile strength values than PBT/SF composites, but also yielded a more stable tensile strength when the SF content was above 20 wt%. This can be explained, in part, by the more homogeneous dispersion resulting from the formation of branched or cross-linked macromolecules of SF in the PBT-g-AA matrix. Grafting of the AA onto PBT increased the tensile strength of the SF composite.

Thermogravimetric analysis (TGA)

It is known that the defunctionalization of SF can be realized by thermal decomposition. In this study, TGA was used to determine the effect of SF content on the weight loss of the hybrids (Fig. 6; Table 2). For both composites, IDT decreased with increasing SF content. This may be due to the SF-induced expansion of PBT or PBT-g-AA, which produces a slack polymer structure and a reduced IDT.

At the same SF content, the PBT-g-AA/SF composites displayed a higher IDT than the PBT/SF composites (Fig. 6; Table 2). This reduced IDT was most likely caused by the increased difficulty in polymer chain arrangement, due to the prohibition of polymer segment movement by SF. Other potential causes include the condensation reaction, which leads to the increased adhesion of SF with PBT-g-AA. These results are similar to those obtained with composites of polyester and other

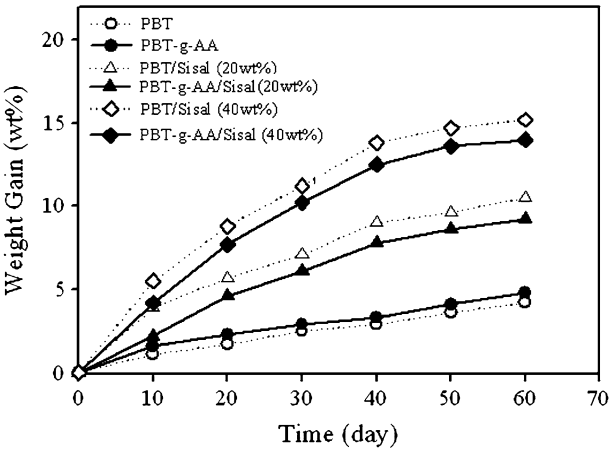

Fig. 7 Percentage weight gain due to water absorption for PBT/SF and PBT-g-AA/SF composites

natural fibers [10, 23]. This outcome is a result of the difference in interfacial forces between the two hybrids: specifically, the weaker hydrogen bonds of PBT/SF compared with the stronger coordination sites associated with the carboxyl groups of PBT-g-AA/SF. The values of IDT in PBT-g-AA/SF were approximately 4–8 °C higher than those of PBT/SF. These higher IDT values were most likely due to the formation of the ester carbonyl groups.

Figure 6 shows the residual mass curves for PBT, PBT-g-AA, PBT/SF, and PBT-g-AA/SF. The PBT/SF or PBT-g-AA/SF exhibit a higher thermal resistance than the PBT or PBT-g-AA due to the content of SF. In addition, the percentage of residual mass at the end of the assessment was higher for the SF matrix, indicating that it forms a charring structure [10, 23].

Water absorption

At the same SF content, the PBT-g-AA/SF composites exhibited a higher water resistance than the PBT/SF composites (Fig. 7). The water resistance of the PBT-g-AA/SF composites was moderate, and it is proposed that the interaction of PBT-g-AA with SF increased the hydrophobicity of SF in these composites. For both PBT/SF and PBT-g-AA/SF, the percentage water gain over the 60-day test period increased with increasing SF content. Because the polymer chain exists in a presumably random arrangement, this seems likely to be the result of increased difficulty in forming an ordered chain configuration with higher levels of SF, and the hydrophilic character of SF, which adheres weakly to the more hydrophobic PBT.

Biodegradation in soil

Changes in the morphology of both the PBT and PBT-g-AA/SF composites were noted as a function of the time they were buried in soil. SEM photomicrographs

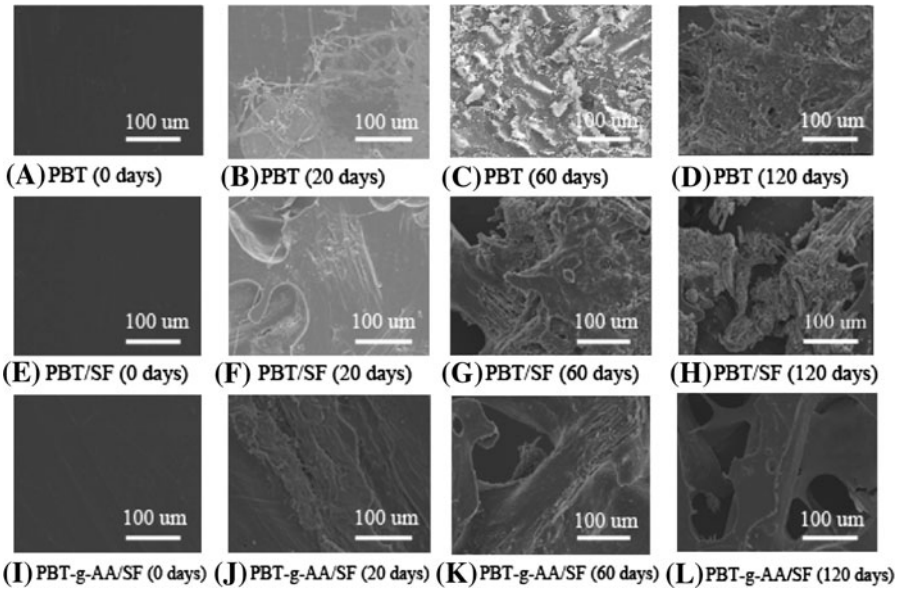

Fig. 8 SEM micrographs show the morphology of PBT (**a–d**), PBT/SF (**e–h**), and PBT-g-AA/SF (**i–l**) films as a function of the soil incubation period

taken after 20, 60, and 120 days illustrate the extent of morphological changes (Fig. 8). PBT/SF (20 wt%; Fig. 8f–h) exhibited larger and deeper pits that appeared more randomly distributed than those in the PBT-g-AA/SF (20 wt%) composites (Fig. 8j–l). These analyses also indicated that the biodegradation of the SF phase in PBT/SF (20 wt%) increased with time (Fig. 9).

Following a 2-week incubation period, cell growth with gradual erosion and cracking was observed on the surface of the PBT matrix (Fig. 8b). After 6 weeks, disruption of the PBT matrix became more apparent (Fig. 8c). This degradation was confirmed by the increasing weight loss of the PBT matrix as a function of incubation time (Fig. 9), which reached nearly 10% after only 120 days. The most likely cause of this weight loss was biodegradation.

The SEM photomicrographs in Fig. 8 indicate that the PBT-g-AA/SF (20 wt%) composites were more readily degraded than neat PBT. Following a 20-day incubation period, the PBT-g-AA/SF composite was coated with a biofilm of bacterial cells (Fig. 8j), indicating more cell growth than that observed on PBT at the same incubation time. Moreover, at 60 and 120 days, larger pores were apparent in the PBT-g-AA/SF composite (Fig, 8k, l), indicating a higher level of degradation. The rate of weight loss of the PBT-g-AA/SF composites was also accelerated relative to that of PBT, exceeding 20% after 120 days (Fig. 9). These results demonstrate that the addition of SF to the PBT-g-AA enhanced the biodegradability of the composite.

Figure 9 shows the percentage weight change as a function of time for the PBT/SF and PBT-g-AA/SF composites buried in the soil compost. For both composites, the degree of weight loss increased with increasing SF content.

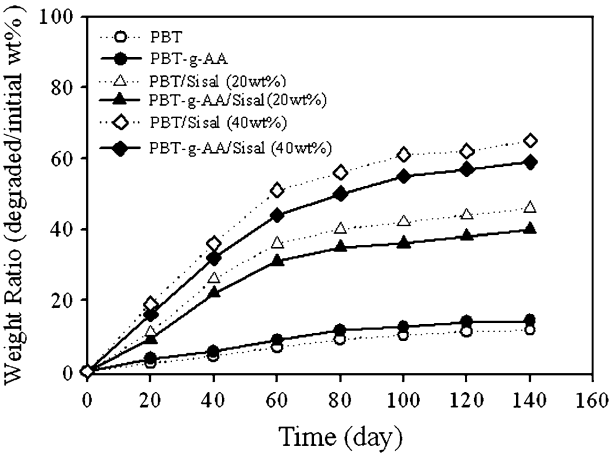

Fig. 9 Weight loss percentages of PBT, PBT-g-AA, PBT/SF, and PBT-g-AA/SF are shown as a function of the incubation time in soil

Composites with 40 wt% SF degraded rapidly over the first 6 weeks, losing a mass approximately equivalent to their SF content, and showed a gradual decrease in weight over the next 60 days. PBT-g-AA/SF exhibited a weight loss of approximately 2–10 wt%.

Conclusions

In this study, the compatibility and mechanical properties of SF blended with PBT and AA-modified PBT (PBT-g-AA) were examined. FTIR and NMR analyses revealed that the formation of ester groups from the reaction between the –OH groups in SF and the anhydride carboxyl groups in PBT-g-AA significantly altered the structure of the composite material. The morphology of the PBT-g-AA/SF composites was consistent with good adhesion between the SF phase and the PBT-g-AA matrix. In mechanical tests, AA grafting enhanced the mechanical properties of the composite, particularly the tensile strength. Although the water resistance of PBT-g-AA/SF was higher than that of PBT/SF, the rate of PBT-g-AA/SF biodegradation was slower than that of PBT/SF, but faster than that of pure PBT, when incubated in soil. After 120 days, the PBT-g-AA/SF (40 wt%) composite suffered >50% weight loss. The degree of biodegradation increased with increasing SF content.

Acknowledgments The author thanks the National Science Council (Taipei City, Taiwan, R.O.C.) for financial support (NSC 99-2622-E-244-001-CC3).

References

1. Satyanarayana KG, Arizaga GGC, Wypych F (2009) Biodegradable composites based on lignocellulosic fibers—an overview. Prog Polym Sci 34:982–1021

2. Steinbüchel A (2005) Non-biodegradable biopolymers from renewable resources: perspectives and impacts. Curr Opin Biotechnol 16:607–613
3. Yu L, Dean K, Li L (2006) Polymer blends and composites from renewable resources. Prog Polym Sci 31:576–602
4. Tripathy AR, Chenl W, Kukureka SN, MacKnight WJ (2003) Novel poly(butylene terephthalate)/poly(vinyl butyral) blends prepared by in situ polymerization of cyclic poly(butylene terephthalate) oligomers. Polymer 44:1835–1842
5. Xiao J, Hu Y, Yang L, Cai Y, Song L, Chen Z, Fan W (2006) Fire retardant synergism between melamine and triphenyl phosphate in poly(butylene terephthalate). Polym Degrad Stab 91: 2093–2100
6. Loua CW, Lin CW, Lei CH, Su KH, Hsu CH, Liu ZH, Lin JH (2007) PET/PP blend with bamboo charcoal to produce functional composites. J Mater Process Technol 192–193:428–433
7. Kunanopparat T, Menut P, Morel MH, Guilbert S (2008) Reinforcement of plasticized wheat gluten with natural fibers: from mechanical improvement to deplasticizing effect. Composites A 39:777–785
8. Chow CPL, Xing XS, Li RKY (2007) Moisture absorption studies of sisal fibre reinforced polypropylene composites. Compos Sci Technol 67:306–313
9. Velde KV, Kiekens P (2001) Thermoplastic pultrusion of natural fibre reinforced composites. Compos Struct 54:355–360
10. Lei Y, Wu Q, Yao F, Xu Y (2007) Preparation and properties of recycled HDPE/natural fiber composites. Composites A 38:1664–1674
11. Coulembiera O, Dege'ee P, Hedrickb JL, Dubois P (2006) From controlled ring-opening polymerization to biodegradable aliphatic polyester: especially poly(β-malic acid) derivatives. Prog Polym Sci 31:723–747
12. Liang D, Hsiao BS, Chu B (2007) Functional electrospun nanofibrous scaffolds for biomedical applications. Adv Drug Deliv Rev 59:1392–1412
13. Ríhová B (1996) Biocompatibility of biomaterials: hemocompatibility, immunocompatiblity and biocompatibility of solid polymeric materials and soluble targetable polymeric carriers. Adv Drug Deliv Rev 21:157–176
14. Wu CS (2005) Improving polylactide/starch biocomposites by grafting polylactide with acrylic acid—characterization and biodegradability assessment. Macromol Biosci 5:352–361
15. Alvarez VA, Ruseckaite RA, Va′zquez A (2006) Degradation of sisal fibre/Mater Bi-Y biocomposites buried in soil. Polym Degrad Stab 91:3156–3162
16. Su WY, Wang Y, Min K, Quirk RP (2001) In situ copolymerization and compatibilization of polyester and polystyrene blends. I. Synthesis of functionalized polystyrenes and the reactions with polyester. Polymer 42:5107–5119
17. Wu CS (2008) Evaluation of polybutylene succinate (PBSU)/starch and PBSU-g-AA/starch composites as capsule material for controlled release of phosphate-solubilizing Bacillus fertilizer. J Control Release 132:42–48
18. Shah BL, Selke SE, Walters MB, Heiden PA (2008) Effects of wood flour and chitosan on mechanical, chemical, and thermal properties of polylactide. Polym Compos 29:655–663
19. Jansen MAG, Goossens JGP, Wit G, Bailly C, Koning CE (2006) The microstructure of poly(butylene terephthalate) copolymers via ^{13}C NMR sequence distribution analysis: Solid-state copolymerization versus melt copolymerization. Anal Chim Acta 557:19–30
20. Martins MA, Forato LA, Mattoso LHC, Colnago LA (2006) A solid state ^{13}C high resolution NMR study of raw and chemically treated sisal fibers. Carbohydr Polym 64:127–133
21. Wu CS (2004) Analysis of mechanical, thermal, and morphological behavior of polycaprolactone/wood flour blends. J Appl Polym Sci 94:1000–1006
22. Raquez JM, Nabar Y, Narayan R, Dubois P (2008) Novel high-performance talc/poly[(butylene adipate)-*co*-terephthalate] hybrid materials. Macromol Mater Eng 293:310–320
23. Luyt AS, Malunka ME (2005) Composites of low-density polyethylene and short sisal fibres: the effect of wax addition and peroxide treatment on thermal properties. Thermochim Acta 426:101–107